Thin Solid Films 517 (2009) 6069–6075

Contents lists available at ScienceDirect

Thin Solid Films

journal homepage: www.elsevier.com/locate/tsf

Influence of acetic acid and ammonia catalyst on microstructure and properties of fluorinated polyimide–organosilicate hybrids

Tzu Hsuan Chiang [a], Szu-Ling Liu [b,1], Shyh-Yang Lee [b,2], Tsung-Eong Hsieh [b,*]

[a] Department of Environment Engineering, Chin Min Institute of Technology, 110, Syuefu Rd., Toufen Township, Miaoli County 351, Taiwan, ROC
[b] Department of Materials Science and Engineering, National Chiao Tung University, 1001, Ta-Hsueh Rd., Hsinchu, 300, Taiwan, ROC

ARTICLE INFO

Article history:
Received 20 August 2008
Received in revised form 1 May 2009
Accepted 11 May 2009
Available online 15 May 2009

Keywords:
Polyimide–organosilicate hybrids
Sol–gel process
Catalyst
Xerogel
Electrical properties

ABSTRACT

This work investigates the preparation, microstructure and thermal/electrical properties of fluorinated polyimide–organosilicate hybrids utilizing acetic acid and ammonia as the catalysts for sol–gel process to grow organosilicate filler particles. Nano-scale organosilicate was observed in the base-catalyzed hybrids, which was ascribed to the relative inertness of base catalysts in promoting the hydrolysis reaction. This postponed the formation of particles and hence smaller particle size. Electrical measurements found that the base-catalyzed hybrids possess lower dielectric constants ($\kappa = 2.40$ at nominal Si content = 0.4 mol) due to the absence of polar groups and formation of silica xerogels with high porosity in the samples. In both hybrids, leakage current densities increase with the increase of Si content. However, leakage current density of base-catalyzed hybrid was higher than that of acid-catalyzed hybrid at the same Si content due to the smaller particle size and highly porous feature of organosilicate embedded in the base-catalyzed hybrids.

1. Introduction

Excellent thermal, mechanical and dielectric properties enable a wide application of polyimides (PIs) in microelectronics; however, relatively high water absorption and the coefficient of thermal expansion somehow limit their applications [1]. A common way to eliminate such deficiencies is to form the composites by adding inorganic fillers such as silica into the polymer matrix to achieve desired physical properties. Nevertheless, the weak interactions between organic and inorganic phases inhibit the compatibility between PIs and silica phase [2]. Many attempts have been made to promote the phase compatibility in PI–silica hybrids [3–8], for example, the introduction of the ethoxysilyl group into the polymer main chain [5,6], blending of proper coupling agents in the precursor solution [7,8].

Recent studies relating to the PI–silica composites containing nano-scale silica particles prepared by sol–gel processes found that the measured densities of samples are lower than the theoretical values [6], featuring the formation of porous structures in the hybrids. Conventional sol–gel processes to form silica fillers involve the hydrolysis of silicon alkoxides and polycondensation of forming compounds. The necessary ingredients include polar solvents, strong inorganic acids, catalysts and water. Hydrolysis and condensation of tetramethoxysilane, tetraethoxysilane (TEOS) or sodium silicate precursor in the presence of an acid or a base catalyst trigger the cross-linking reactions to form the amorphous SiO_2 [9,10]. Catalysis conditions are known to affect the microstructures of silica sols that may eventually affect the physical properties of hybrids. For sol–gel reactions, hydrochloric acid (HCl) is the most common inorganic acid catalyst [10–13] while the organic acid catalysts include the citric acid ($C_6H_8O_7$) and acetic acid (CH_3COOH) [14,15]. The adoption of acetic acid as catalyst is due to its ease dissolution in a wide variety of precursors, enabling a multitude of multi-cation solutions [16]. On the other hand, the base chemicals such as ammonia (NH_4OH) may also serve as the catalyst of sol–gel reactions [10,17–19]. For instance, Matsoukas and Gulari found that the ammonia catalyst not only affects the hydrolysis reaction but also promotes the polymerization rate in the sol–gel process for growing colloidal silica particles [19]. This resulted in a faster growth kinetics and hence larger silica particles.

In this study, acetic acid and ammonia are adopted as the catalysts for sol–gel reaction utilizing TEOS and diethoxydimethylsilane (DEDMS) as the precursors. The resulted organosilicate particles are then implanted in fluorinated PI to form the hybrid samples and the relationships between microstructure and thermal/electrical properties are investigated. The effects of acid-catalyzed and base-catalyzed sol–gel processes on silica particle formation and its geometry features in hybrid sample are also discussed.

2. Experimental details

2.1. Materials

For the preparation of fluorinated PI, 4,4′-diamiodiphenylether (ODA) was supplied by Merck-Schuehardt Co.; *n*,*n*-dimethylacetamide

* Corresponding author.
E-mail address: tehsieh@mail.nctu.edu.tw (T.-E. Hsieh).
[1] Currently at Taiwan Semiconductor Manufacturing Company (TSMC), Ltd., Taiwan, ROC.
[2] Currently at Golden View Technology Company, Ltd., Taiwan, ROC.

0040-6090/$ – see front matter © 2009 Elsevier B.V. All rights reserved.
doi:10.1016/j.tsf.2009.05.013

Table 1
A list of molar numbers of ingredients for the preparation of organosilicate-A and organosilicate-B precursors for various hybrid samples.

Precursors[a]	Sample[b]	Nominal Si content[c] (mole)	TEOS (mole)	DEDMS (mole)	H_2O (mole)	EtOH (mole)	CH_3COOH (mole)	NH_4OH (mole)
Organosilicate-A	HASi0.2	0.2	0.133	0.067	0.333	2.660	0.200	–
	HASi0.3	0.3	0.200	0.100	0.500	4.000	0.300	–
	HASi0.4	0.4	0.266	0.134	0.665	5.320	0.400	–
	HASi0.5	0.5	0.333	0.167	0.833	6.667	0.500	–
	HASi0.6	0.6	0.400	0.200	1.000	8.000	0.600	–
	HASi0.7	0.7	0.466	0.234	1.165	9.320	0.700	–
	HASi0.8	0.8	0.532	0.268	1.330	10.640	0.800	–
Organosilicate-B	HBSi0.2	0.2	0.133	0.067	0.333	2.660	–	0.067
	HBSi0.3	0.3	0.200	0.100	0.500	4.000	–	0.100
	HBSi0.4	0.4	0.266	0.134	0.665	5.320	–	0.134
	HBSi0.5	0.5	0.333	0.167	0.833	6.667	–	0.167
	HBSi0.6	0.6	0.400	0.200	1.000	8.000	–	0.200
	HBSi0.8	0.8	0.532	0.268	1.330	10.640	–	0.268

[a] Initially, 2 mol of PAA was prepared, then the above ingredients were added to form the organosilicate-A and organosilicate-B precursors.
[b] The samples are denoted by HXSiY in which X represents the hybrid type (X = A for acid catalyst or B for base catalyst) while Y represents the nominal Si content in mole (Y = 0.2 to 0.8).
[c] The sum of mole numbers of TEOS and DEDMS is defined as the nominal Si content of hybrid sample.

(DMAc) was purchased from ACROS Co.; hexafluoroisopropylidene-2,2-bisphthalic dianhydride (6FDA) was provided by CHRISKEV Company, Inc. For the preparation organosilicate, TEOS was supplied by TEDIA Co. and diethoxydimethylsilane, DEDMS was provided by Lancaster Co. Acetic acid was provided by SHIMAKYO Co. Ammonia was provided by WAKO PURE Chemicals Industries, Ltd. Ethanol (EtOH) was supplied by SHOWA Chemicals Inc. All chemicals are with 99% purity.

2.2. Preparation of poly(amic acid) precursor

The poly(amic acid) (PAA) precursors for fluorinated PI were prepared by first dissolving ODA in DMAc at the molar ratio = 1:1 in nitrogen ambient. After soaking in an ice bath for 10 min, 6FDA was slowly added into the mixture at 6FDA:ODA molar ratio = 1:1. After the removal of ice bath, both mixtures were left alone in room temperature and continuously stirred for 8 h to yield the PAA precursor solutions with solid contents = 20 wt.%, respectively.

2.3. Preparation of PI–organosilicate hybrids

The acid-catalyzed organosilicate (organosilicate-A) and base-catalyzed organosilicate (organosilicate-B) precursors were prepared in acetic acid and ammonia solution *via* sol–gel process, respectively. The hydrolysis and condensation reactions were carried out at $R = 0.5$ (R = the molar ratio of water *versus* the molar ratio of organic functional groups of TEOS and DEDMS for hydrolysis), TEOS:DEDMS:H_2O:EtOH:CH_3COOH (in molar ratio) = 1:0.5:2.5:20:1.5 and TEOS:DEDMS:H_2O:EtOH:NH_4OH (in molar ratio) = 1:0.5:2.5:20:0.5. The molar numbers of above ingredients for the preparation of organosilicate-A and organosilicate-B precursors are listed in Table 1 and in this work the sum of mole numbers of TEOS and DEDMS is defined as the nominal Si content of hybrid samples.

Afterward, the organosilicate-A and organosilicate-B precursors were mixed with PAA precursors, respectively, then stirred for 12 h at room temperature in nitrogen ambient to form the fluorinated PAA–organosilicate-A and PAA–organosilicate-B precursors. The precursors containing various amounts of TEOS/DMDES were prepared so as to yield the hybrid samples with various nominal Si contents.

The fluorinated PI–organosilicate hybrid samples were prepared as follows. First, the PAA–organosilicate-A or PAA–organosilicate-B precursor was spin coated on appropriate substrates. A soft baking at 90 °C for 10 min followed by a curing treatment with temperature profile shown in Fig. 1 was then preformed so as to form the PI–organosilicate-A (termed as HA hereafter) and PI–organosilicate-B (termed as HB hereafter) hybrid thin film samples. Below, the symbol for hybrid sample is designated as HXSiY in which X represents the catalyst type (X = A for acid catalyst or B for base catalyst) while Y represents the nominal Si content in mole (Y = 0.2 to 0.8 for both types of hybrids).

2.4. Infrared spectroscopy

The samples for Fourier transform infrared spectroscopy (FTIR) were prepared by spin coating the precursors on KBr discs. The FTIR measurements were performed on the samples subjected to the soft baking and curing treatment described previously. The FTIR spectra of samples were obtained by a Nicolet Protégé™-460 FTIR spectrometer in the wavenumber range of 400 to 4000 cm^{-1} with the spectral resolution = 4 cm^{-1}.

2.5. Solid-state ^{29}Si Nuclear Magnetic Resonance Spectroscopy (^{29}Si NMR)

The fluorinated PI–organosilicate samples prepared were *via* the soft baking and curing process shown in Fig. 1. They were then cut into small pieces and then sent to a Bruker DSX400WB NMR to characterize their ^{29}Si NMR spectra.

2.6. Thermogravimetric Analysis (TGA)

The 10% weight loss decomposition temperature (T_d) was measured by using a thermogravimetric analyzer (Du Pont Instruments TGA

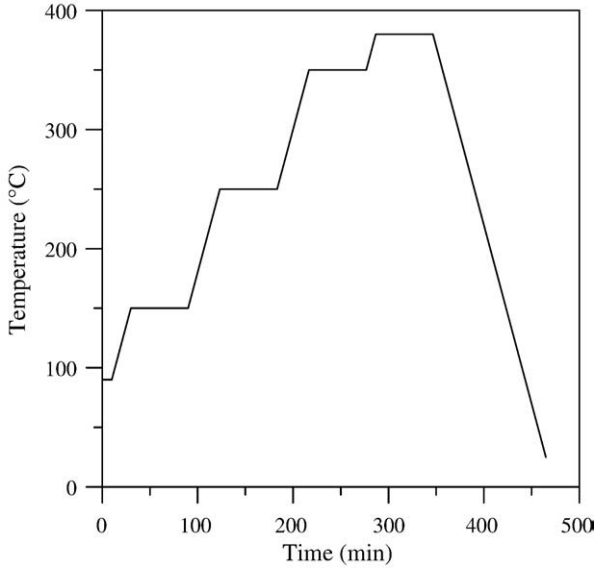

Fig. 1. Temperature profile of curing process for fluorinated PI–organosilicate hybrids.

2950) from room temperature to 900 °C at a heating rate of 10 °C/min in nitrogen ambient. The TGA analysis was also carried in air ambient so as to obtain the residual weight of inorganic content.

2.7. Morphology characterizations

The morphologies of the fracture surface of the hybrid samples were examined by using a scanning electron microscope (SEM, Jeol JSM-633F FEG-SEM, Japan). For the preparation of transmission electron microscope (TEM) samples, the precursor was first spin coated on KBr disc and subsequently cured according to the process shown in Fig. 1. After dissolving the KBr away in deionized water, the hybrid layer was mounted on the Cu mesh and then sent to a JEOL 2000FX STEM operating at 200 kV for microstructure characterization.

2.8. Electrical properties

The samples with the structure of Al (500 nm)/hybrid layer (500 to 600 nm)/Pt (150 nm)/Si substrate were prepared for electrical property measurements. The relative dielectric constants (k) of hybrid samples were deduced from the measurement using an HP 4280A capacitance meter at a frequency of 1 MHz. The current–voltage (I–V) characteristics of the samples were obtained by an HP 4156B semiconductor parameter analyzer at the applied bias field ranging from 0 to 1.5 MV/cm.

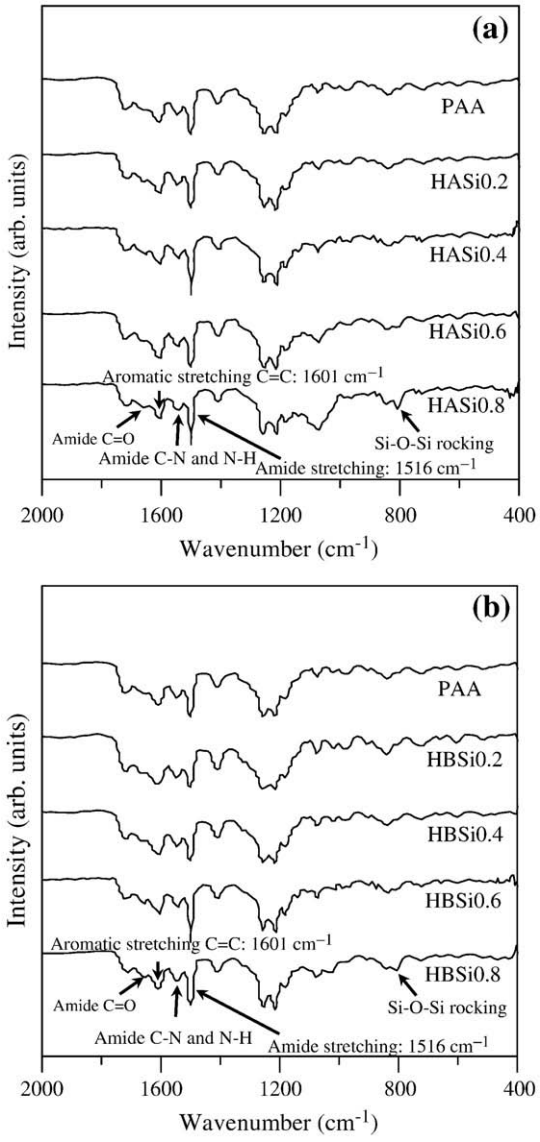

Fig. 2. FTIR spectra of (a) PAA–organosilicate-A and (b) PAA–organosilicate-B precursors with various nominal Si contents subjected to soft baking treatment at 90 °C for 10 min.

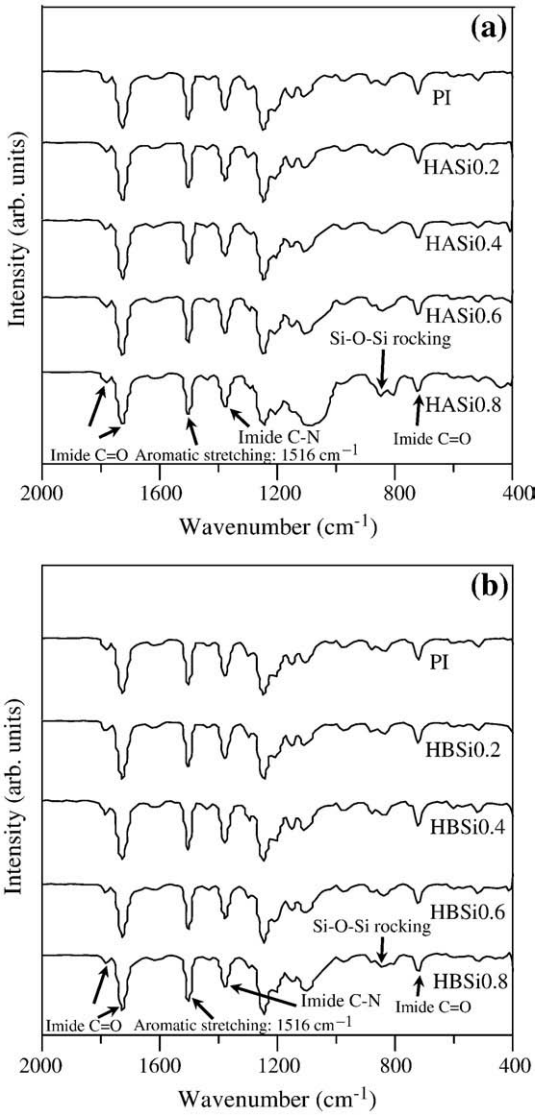

Fig. 3. FTIR spectra of cured (a) PI–organosilicate-A and (b) PI–organosilicate-B hybrids with various nominal Si contents.

3. Results and discussion

3.1. FTIR analysis

Fig. 2(a) and (b) shows the FTIR spectra of HA and HB hybrids with various nominal Si contents subjected to soft baking treatment. Formation of organosilicate is deduced by the absorption bands appearing at around 804 cm^{-1} for Si–O–Si symmetric rocking and stretching vibrations, evidencing the occurrence of hydrolysis reaction of TEOS and DEDMS [8]. Fig. 2(a) and (b) also indicates that the peak at 1656 cm^{-1} corresponding to C=O of amides and the peak at 1543.5 cm^{-1} corresponding to combination absorbance of N–H and C–N of amides emerge for the hybrid samples prior to curing. However, for the cured hybrid samples, the occurrence of imidization is evidenced by the peaks at 1781 cm^{-1} (asymmetric stretching C=O

of imide), 1720 cm^{-1} (symmetric C=O stretching of imide), 1380 cm^{-1} peak (C–N stretching of imide) and 725 cm^{-1} (C=O bending of imide) as shown in Fig. 3(a) and (b), respectively [20]. We note that the 804 cm^{-1} peak corresponding to Si–O–Si network vibrations is present in all FTIR spectra of cured hybrid samples.

3.2. ^{29}Si NMR analysis

Fig. 4 presents the ^{29}Si NMR spectra of organosilicate derived from pure TEOS and TEOS/DEDMS (molar ratio = 2, $R = 0.5$) *via* the sol–gel reaction. In both cases, the presence of peaks at −110, −101.3 and −91.6 ppm implies the formation of structural units $Si(O_{0.5})_4$ (Q^4, the four bridging bond unit), $(RO)Si(O_{0.5})_3$ (Q^3, the three bridging bond unit) and $(RO)_2Si(O_{0.5})_2$ (Q^2, the two bridging bond unit) [21]. The Q^3 and Q^2 peaks indicate that the incomplete hydrolysis resulted from the uncondensed silanol in organosilicate. For TEOS/DEDMS sample, the intensity of peak corresponding to Q^4 unit at −110 ppm is obviously higher, indicating a more complete hydrolysis in comparison with pure TEOS [22]. Furthermore, an extra peak at −12.61 ppm appears in the case of TEOS/DEDMS. It implies the presence of $-(CH_3)_2SiO-$ functional group (*i.e.*, the *D* unit) in organosilicate [23] due to the addition of DEDMS.

Fig. 5 presents the ^{29}Si NMR spectra of acid- and base-catalyzed PI–organosilicate hybrids. The Q^4 units dominate the structure of organosilicate in both types of hybrids, illustrating that more tetra-substituted siloxanes (*i.e.* the organosilicate) are generated in the hybrids. However, the peak intensity corresponding to Q^4 unit is comparatively less in base-catalyzed hybrid due to the fact that the hydrolysis rate of silicon alkoxides in base-catalyzed condition is slower than that in acid-catalyzed condition. This implies a less amount of organosilicate in base-catalyzed hybrids.

As shown in Fig. 5, the peaks emerging at −16.96 and −18.25 ppm indicate the presence of *D* units in both hybrids. In comparison with Fig. 4, there is an obvious NMR peak shift for the *D* units in hybrid samples. For acid-catalyzed hybrids, this is attributed to the strong hydrogen bonds in the interpenetrating network (IPN) structure formed by the intercalation of PI with Si–OH–Si groups [24] while for base-catalyzed hybrids, the covalent bond in IPN structure formed by the intercalation of PI with lone pair electron of oxygen on Si–O–Si groups during condensation reaction induces the peaks shift [25].

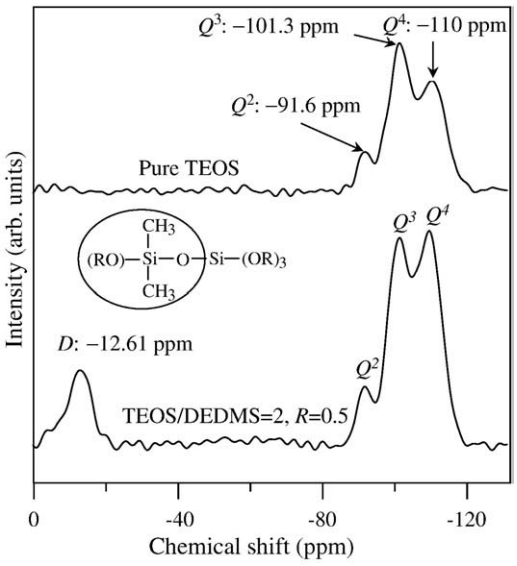

Fig. 4. ^{29}Si NMR spectra of organosilicate derived from pure TEOS and TEOS/DMES = 2 at $R = 0.5$.

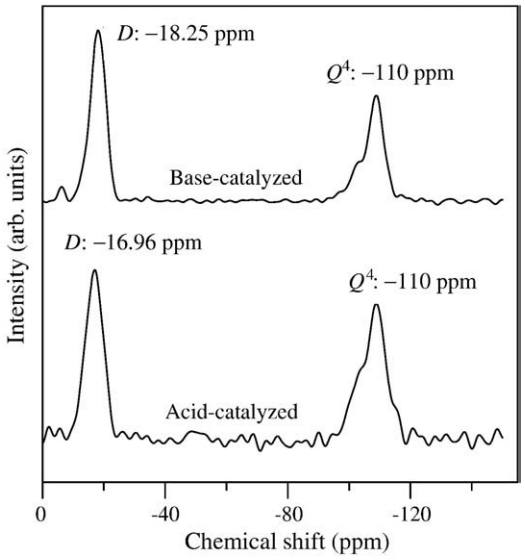

Fig. 5. ^{29}Si NMR spectra of acid- and base-catalyzed PI–organosilicate hybrids.

3.3. Thermal properties

The thermal properties of PI–organosilicate-A and PI–organosilicate-B hybrids containing various amounts of Si contents evaluated by TGA are listed in Table 2. It can be seen that regardless of the ambient type of TGA analysis, the T_d of sample increases with the increase of Si content. This indicates that the implantation of organosilicate fillers benefits the thermal stability of hybrids, a result similar to that reported in the study of phenolic/silica nanocomposites [26]. We note that all hybrids exhibit inferior thermal stability in air ambient, indicating that the organo groups of organosilicate are less stable in oxygen environment. Furthermore, for the sample at the same Si content, the T_d of PI–organosilicate-B hybrid was higher than that of PI–organosilicate-A hybrid. This is ascribed to the fact that the Si–O–Si group provides a stronger interaction between organosilicate particles and PI in the base-catalyzed hybrids [6] which, in turn, inhibits the polymer degradation and thus increases the T_d of hybrid [27].

Table 2 also lists the residual weight percentage (R_c) of hybrids heated up from room temperature to 900 °C in air and it can be seen that the value of R_c increases with the increase of Si content in the hybrids. Further, the R_c for acid-catalyzed sample is higher than that of base-catalyzed sample at the same Si content. This is due to the high hydrolysis rate in acid-catalyzed hybrids which results in the high amount of organosilicate formed in the samples [8]. We note that the analytical results of R_c are in good agreement with the NMR results presented in Fig. 5.

Table 2
Thermal properties of PI–organosilicate hybrids evaluated by TGA.

Sample	Nominal Si content (wt.%)	T_d (°C) in N_2	T_d (°C) in air	R_c (wt.%)
Pure PI	0	567	561	0.11
HASi0.2	2.41	564	556	0.65
HASi0.3	4.05	564	553	1.00
HASi0.4	6.17	567	554	1.97
HASi0.5	8.98	569	549	1.26
HASi0.6	12.89	577	551	5.38
HASi0.7	18.71	581	552	10.19
HASi0.8	28.29	585	554	19.03
HBSi0.2	2.41	565	556	0.15
HBSi0.3	4.05	574	563	0.29
HBSi0.4	6.17	581	566	0.39
HBSi0.5	8.98	582	565	0.43
HBSi0.6	12.89	588	568	0.90
HBSi0.8	28.29	592	569	1.76

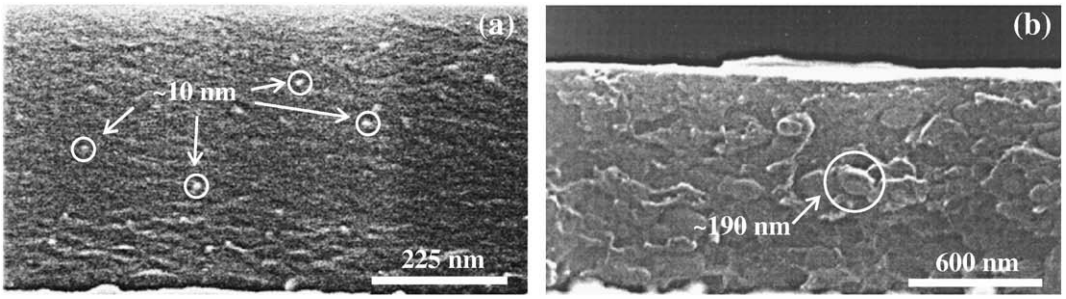

Fig. 6. SEM micrographs of fracture surfaces of acid-catalyzed hybrid samples: (a) HASi0.4 and (b) HASi0.8.

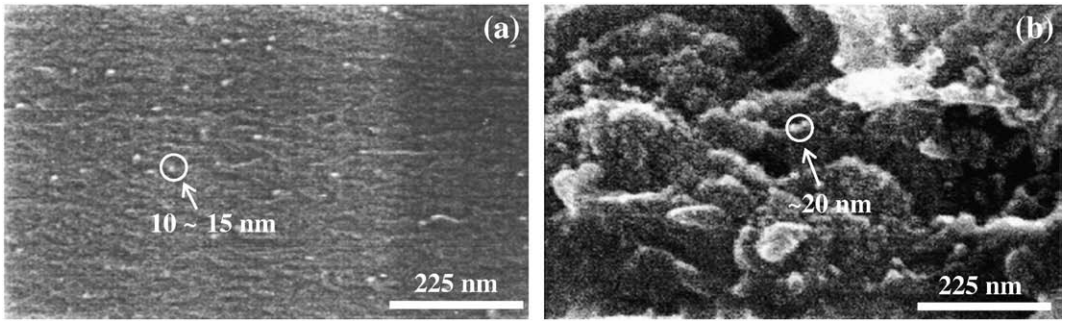

Fig. 7. SEM micrographs of fracture surfaces of base-catalyzed hybrid samples: (a) HBSi0.4 and (b) HBSi0.8.

3.4. Morphology characterizations

Figs. 6(a)–(b) and 7(a)–(b) present the SEM micrographs of the fractured surface of acid- and base-catalyzed hybrids with 0.4 and 0.8 mol Si contents, respectively. In acid- and base-catalyzed samples, the organosilicate particle sizes with ≤10 nm are observed when Si content ≤0.4 mol whereas, as shown in Fig. 6(b), apparent particle coarsening occurs in acid-catalyzed sample with high Si content (*e.g.*, HASi0.8). A further TEM characterization on HASi0.8 and HBSi0.8 samples confirms above SEM results that, as shown in Fig. 8(a) and (b), the organosilicate particle sizes of acid-catalyzed are in the range of 175 to190 nm while those in the base-catalyzed hybrid are in the range of 10 to 40 nm. Furthermore, according to the TEM micrographs shown in Fig. 8, the sizes of particles in acid-catalyzed hybrids seem to be more uniform in comparison with those in base-catalyzed samples. Thitinuna et al. reported similar results that the spirosilicates formed under HCl-catalyzed condition exhibit a larger particle size in comparison with that formed under NH_4OH-catalyzed condition [28]. The TEOS has a relatively strong electron-donating alkyl group which prefers to react with the acid catalyst during hydrolysis [29]. Therefore, the hydrolysis rate of acid-catalyzed process was higher than that of base-catalyzed process. Meanwhile, the particles formed tend to be large in size due to the formation of hydroxylated monomer *via* electrophilic reactions, providing more chain ends for the formation of extended, highly branched linear particles during condensation reaction [30]. On the contrary, the base catalyst is less active in promoting the hydrolysis reaction that the repulsion of sol structure postpones the formation of particles and hence the smaller particle sizes.

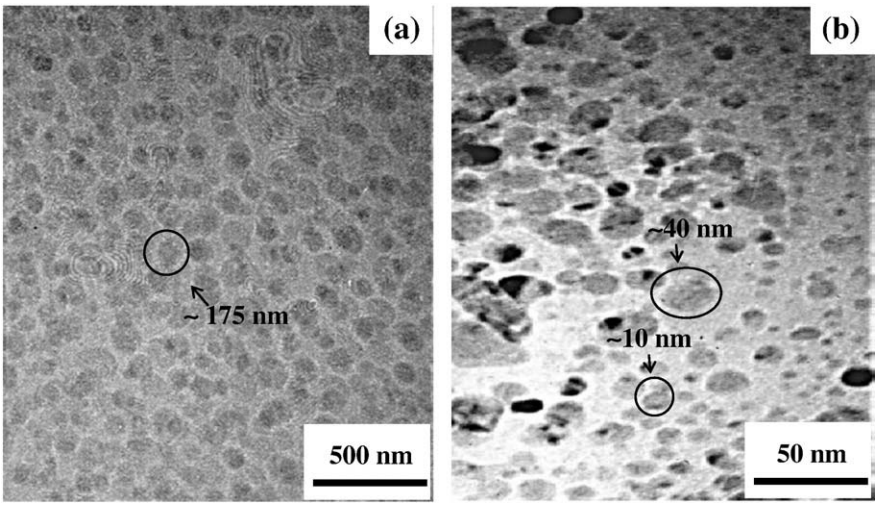

Fig. 8. TEM micrographs of (a) HASi0.8 and (b) HBSi0.8 hybrid samples.

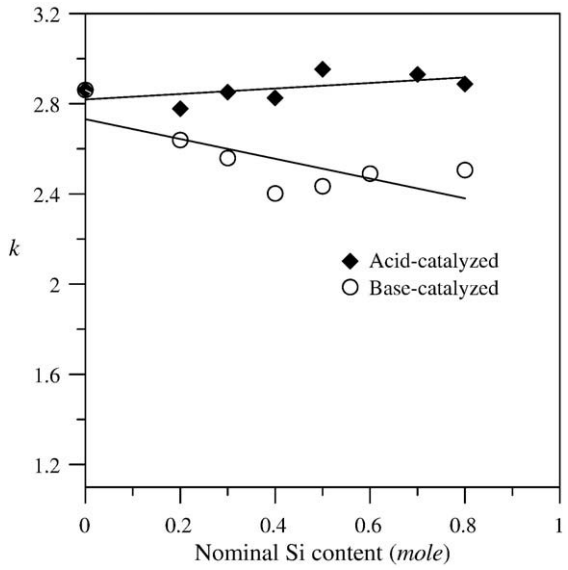

Fig. 9. The dielectric constants of acid- and base-catalyzed PI–organosilicate hybrids as a function of nominal Si content.

However, the base-catalyzed reaction takes place *via* nucleophilic attack and the condensation reaction is able to provide the SiO^-, inducing a faster condensation before the completion of hydrolysis [28].

3.5. Electrical properties

Fig. 9 presents the dielectric constants of acid- and base-catalyzed PI–organosilicate hybrids as a function of nominal Si content. It can be seen that the dielectric constants for base-catalyzed hybrids decrease monotonously with the increase of Si contents whereas, for acid-catalyzed hybrids, though with a slightly increasing trend, the dielectric constants nearly remain the same as that of pristine fluorinated PI.

The suppression of dielectric constant in base-catalyzed hybrids is attributed to the strong interaction between organosilicate particles and the PI matrix in which the Si–O–Si group at the organic–inorganic interfaces effectively restricts the motions of polar functional groups. Further, the hybrid incorporated with nano-scale fillers means more interfacial sites for intercalations and hence the motion constraint of polar functional groups would become more effective. As to the acid-catalyzed hybrids, the inferior dielectric constants can be understood in terms of the following arguments. According to the studies on the reaction mechanisms of sol–gel process, the utilization of TEOS/DEDMS precursor and acetic acid catalyst might result in the reaction with residual methanol to form the volatile methyl acetate ($CH_3COOOCH_3$) and H_2O during hydrolysis [15,31,32]. The polar feature of H_2O would then deteriorate the dielectric properties of hybrid. During the condensation reaction using acid as the catalyst, the polar functional groups such as *R*OH are present and they may raise the dielectric constant of the acid-catalyzed hybrid. The acid-catalyzed hybrids hence exhibit an inferior dielectric property in comparison with the base-catalyzed hybrids.

In this study, the dielectric constant of fluorinated PI free of silica filler is 2.87 and the silica is known to have the dielectric constant of about 4. Hence, according to the principle of composites, the dielectric constants of PI–silica composites should be in the range of 2.87 to 4. However, Fig. 9 shows the decrease of dielectric constant for the base-catalyzed hybrids and the negligible increase of dielectric constant for the acid-catalyzed hybrids. It was hence speculated that the organosilicate embedded in the hybrids might be in a form of porous structure which effectively suppresses the increment of dielectric constants of hybrids. In terms of the measured values of *k*, we calculated the porosities for the cases of silica xerogel and aerogel in

Table 3
The dielectric constants, calculated densities and porosities of acid- and base-catalyzed PI–organosilicate hybrids with various nominal Si content.

Sample	k	ρ_1[a] (g/cm^3)	ρ_2[b] (g/cm^3)	Porosity[c] Π_1, (%)	Porosity[c] Π_2, (%)
PI	2.87	–	–	–	–
HASi0.2	2.78	1.46	1.11	38.74	30.47
HASi0.3	2.86	1.39	1.16	36.05	27.42
HASi0.4	2.83	1.45	1.14	37.02	28.52
HASi0.5	2.95	1.43	1.22	32.78	23.71
HASi0.7	2.93	1.53	1.21	33.47	24.49
HASi0.8	2.89	1.51	1.18	34.95	26.17
HBSi0.2	2.64	1.48	1.03	43.56	35.94
HBSi0.3	2.56	1.28	0.98	46.31	39.06
HBSi0.4	2.40	1.22	0.88	51.82	45.31
HBSi0.5	2.43	1.09	0.89	50.78	44.14
HBSi0.6	2.49	1.12	0.93	48.72	41.80
HBSi0.8	2.51	1.16	0.94	48.03	41.02

[a] $k = 1 + 1.28\rho_1$.
[b] $k = 1 + 1.6\rho_2$.
[c] $\Pi = 1 - \frac{\rho}{\rho_s}$; $\rho_s = 2.27$ g/cm^3 for silica xerogel [33] and $\rho_s = 2.19$ g/cm^3 for silica aerogel [37].

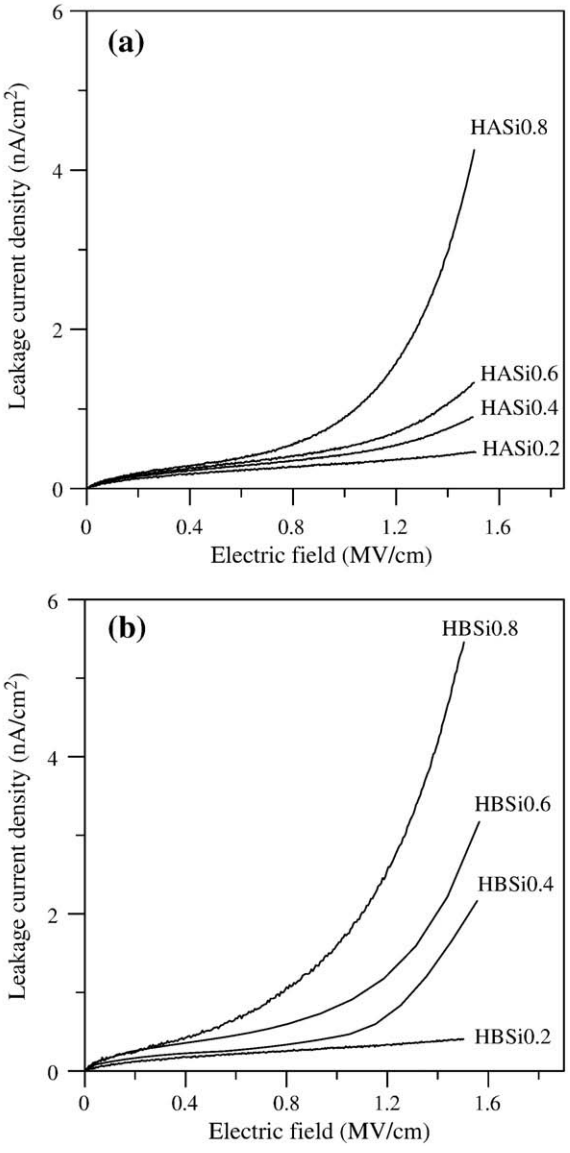

Fig. 10. Leakage current density *versus* applied bias field for (a) acid-catalyzed and (b) base-catalyzed hybrids with various nominal Si contents.

the hybrids by utilizing the formulae proposed by Hong et al. [33] and Hrubesh et al. [34]. It is known that for aerogels, porosity >75%; for xerogels, porosity is <75%; for dense hybrids, porosity <1% [34]. According to the calculated results listed in Table 3, all the values of porosity are less than 75%, implying the plausible formation of silica xerogels in the hybrids.

Further, Table 3 shows that the calculated porosity for base-catalyzed hybrid is higher than that for acid-catalyzed hybrid at the same Si content. This is attributed to the sufficient cross-link occurring in acid-catalyzed sol–gel reactions, implying a dense gel and hence low-porosity organosilicate [35]. As to the base-catalyzed sol–gel reactions, the much slower hydrolysis rate result in a uniform network structure in filler particles and thus the high-porosity organosilicate [35,36].

Fig. 10(a) and (b) presents the leakage current densities of acid- and base-catalyzed hybrids *versus* the applied bias field up to 1.5 MV/cm. In addition to the absence of electrical breakdown, Fig. 10(a) and (b) shows that the acid- and base-catalyzed hybrids both exhibit low leakage current densities at the order of magnitude of 10^{-9} A/cm^2, which is comparable to those of popular low-κ dielectrics such as porous organosilicate glasses [38], aromatic hydrocarbon polymer [39], hydrogen silsesquioxanes [40,41] and methyl silsesquioxanes [42] at the same bias filed. Apparently, the embedment of organosilicate in polymeric matrix may effectively block the migration of charge carriers. Further, the leakage current density increases with the increase of Si content for both types of hybrids and the leakage current density of base-catalyzed hybrid is higher than that of acid-catalyzed hybrid at the same Si content. This is ascribed to the smaller particle size and high-porosity features of organosilicate in the base-catalyzed hybrids. The small size of organosilicate fillers implies a large amount of organosilicate/PI interfaces in the hybrids. Interface is a well-known planar defect that disrupts the continuity of chemical bonds. The dangling bonds at such a structural discontinuity may thus serve as the paths for charge carrier transport. Hence, the high leakage current density was observed in the sample with base-catalyzed hybrid, in particular, when the Si content is high. Yu et al. reported that there are more Si–C bonds with lonely electron pairs in highly porous thin film sample [43]. This might similarly occur in our samples with high Si content and thereby result in the high leakage current density.

4. Conclusions

This work investigates the preparation, microstructure and thermal/electrical properties of fluorinated PI–organosilicate hybrids *via* the acid- and base-catalyzed sol–gel process. Structure analyses revealed the dominance of Q^4 units or, the four bridging bond unit, in the structure of organosilicate. Further, the *D* units were observed due to the strong hydrogen bonds in the IPN structure formed by the intercalation of PI and Si–O–Si structure in base-catalyzed hybrids and Si–OH–Si structure in acid-catalyzed hybrids, respectively. Stronger intercalation of Si–O–Si group with PI was found to provide better thermal stability and lower dielectric constant property for base-catalyzed hybrids. SEM/TEM characterizations revealed smaller sizes of organosilicate particle in base-catalyzed hybrids (*e.g.*, <40 nm for HBSi0.8 sample) in comparison with that in acid-catalyzed hybrids (*e.g.*, ~190 nm for HASi0.8 sample). The embedment of nano-scale organosilicate particles in base-catalyzed hybrids exaggerated the interfacial intercalations and thus benefited the dielectric property. As illustrated by the porosity calculation, improvement of dielectric constants is also attributed to the formation of porous organosilicate (xerogels) in both hybrids. Leakage current density measurement indicated that the embedment of organosilicate may effectively inhibit the charge carrier migration and the leakage current density of about 1 nA/cm^2 at the bias field of 1.5 MV/cm was obtained in the fluorinated PI–organosilicate hybrids prepared in this work.

Acknowledgement

This work was supported by the National Science Council, Taiwan, ROC, under contract No. NSC94-2216-E-009-026.

References

[1] A.A. Arbash, Z. Ahmad, F.A. Sagheer, A.A.M. Ali, J. Nanomater. 2006 (2006) 1.
[2] Z. Ahmad, J.E. Mark, Chem. Mater. 13 (2001) 3320.
[3] L. Wang, Y. Tian, H. Ding, J. Li, Eur. Polym. J. 42 (2006) 2921.
[4] R. Aziz, J.C. Beamish, Circuit World 24 (1998) 24.
[5] S. Wang, Z. Anhmad, J.E. Mark, Chem. Mater. 6 (1994) 943.
[6] Z.K. Zhu, Y. Yang, J. Yin, Z.N. Qi, J. Appl. Polym. Sci. 73 (1999) 2977.
[7] J.H. Wengrovius, V.M. Powell, J.L. Webb, J. Org. Chem. 59 (1994) 2813.
[8] A. Kioul, L. Mascia, J. Non-Cryst. Solids 175 (1994) 169.
[9] C.M.F. Soares, O.A. Santos, H.F. de Castro, F.F. de Moraes, G.M. Zanin, J. Mol. Catal., B Enzym. 39 (2006) 69.
[10] C.R. Silva, C. Airoldi, J. Colloid Interface Sci. 195 (1997) 381.
[11] P. Musto, G. Ragosta, G. Scarinzi, L. Mascia, Polymer 45 (2004) 1697.
[12] K.A. Vorotilov, V.I. Petrovsky, V.A. Vasiljev, M.V. Sobolevsy, J. Sol–Gel Sci. Technol. 8 (1997) 581.
[13] J.Y. Zhang, I.W. Boyd, Mater. Sci. Semicond. Process. 3 (2000) 345.
[14] B. Karmakar, G. De, D. Kundu, D. Ganguli, J. Non-Cryst. Solids 135 (1991) 29.
[15] N.N. Khimich, B.I. Venzel, L.A. Koptelova, I.A. Drozdova, Russ. J. Appl. Chem. 77 (2004) 290.
[16] R.A. Assink, R.W. Schwartz, Chem. Mater. 5 (1993) 511.
[17] K.D. Kim, H.T. Kim, J. Sol–Gel Sci. Technol. 25 (2002) 183.
[18] M.A.B. Meador, E.F. Fabrizio, F. Ilhan, A. Dass, G. Zhang, P. Vassilaras, J.C. Johnston, N. Leventis, Chem. Mater. 17 (2005) 1085.
[19] T. Matsoukas, E. Gulari, J. Colloid Interface Sci. 124 (1988) 252.
[20] L. Mascia, A. Kioul, Polymer 36 (1995) 3649.
[21] Y. Kim, E. Kang, Y.S. Kwon, W.J. Cho, C. Cho, M. Chang, M. Ree, T. Chang, C.S. Ha, Synth. Met. 85 (1997) 1399.
[22] J. Hedrick, H.J. Cha, R.D. Miller, D.Y. Yoon, H.R. Brown, Macromolecules 30 (1997) 8512.
[23] M. Ree, W.H. Goh, Y. Kim, Polym. Bull. 35 (1995) 215.
[24] C.J. Cornelius, E. Marand, Polymer 43 (2002) 2385.
[25] S.K. Duplock, J.G. Matisons, A.G. Swincer, R.F.O. Warren, J. Inorg. Organomet. Polym. 1 (1991) 361.
[26] C.L. Chiang, C.C.M. Ma, Polym. Degrad. Stab. 83 (2004) 207.
[27] I.C. Schrotter, M.S. Hi, C. Guizard, J. Appl. Polym. Sci. 61 (1996) 2137.
[28] S. Thitinuna, N. Thanabodeekija, A.M. Jamiesonb, S. Wongkasemjita, J. Eur. Ceram. Soc. 23 (2003) 417.
[29] M. Kuniyoshi, M. Takahashi, Y. Tokuda, T. Yoko, J. Sol–Gel Sci. Technol. 39 (2006) 175.
[30] S.M. Jones, J. Non-Cryst. Solids 291 (2001) 206.
[31] E. Stathatos, P. Lianos, Langmuir 19 (2003) 7587.
[32] L.T. Arenas, C.W. Simm, Y. Gushikem, S.L.P. Dias, C.C. Moro, T.M.H. Costa, EV. Benvenutti, J. Braz. Chem. Soc. 18 (2007) 886.
[33] J.K. Hong, H.R. Kim, H.H. Park, Thin Solid Films 332 (1998) 449.
[34] L.W. Hrubesh, L.E. Keene, V.R. Latorre, J. Mater. Res. 8 (1993) 1736.
[35] J. Wang, G. Wu, J. Shen, T. Yang, Q. Zhang, B. Zhou, Z. Deng, J. Sol–Gel Sci. Technol. 18 (2000) 219.
[36] S. Yu, T.K.S. Wong, J. Sol–Gel Sci. Technol. 29 (2004) 57.
[37] S. Goizet, J.C. Schrotter, M. Smaihi, A. Deratani, New J. Chem. 21 (1997) 461.
[38] T.C. Chang, T.M. Tsai, P.T. Liu, C.W. Chen, T.Y. Tseng, Thin Solid Films 469–470 (2004) 383.
[39] P.T. Liu, T.C. Chang, S.T. Yan, C.H. Li, S.M. Sze, J. Electrochem. Soc. 150 (2003) F7.
[40] T.C. Chang, P.T. Liu, T.M. Tsai, F.S. Yeh, T.Y. Tseng, M.S. Tsai, B.C. Chen, Y.L. Yang, S.M. Sze, Jpn. J. Appl. Phys. Part 1 40 (2001) 3143.
[41] G. Yin, Z. Ning, Q. Yuan, C. Ye, Y. Xin, J. Am. Ceram. Soc. 90 (2007) 1943.
[42] T.C. Chang, Y.S. Mor, P.T. Liu, T.M. Tsai, C.W. Chen, S.M. Sze, Y.J. Mei, Thin Solid Films 398–399 (2001) 637.
[43] S. Yu, T.K.S. Wong, X. Huw, K. Pita, Thin Solid Films 462–463 (2004) 311.